Analysis of Radiation-Induced Natural Convection in Rectangular Enclosures

B. W. Webb* and R. Viskanta†
Purdue University, West Lafayette, Indiana

A model has been developed for predicting the volumetric deposition rate of radiant energy from an external source in a vertical fluid layer and the subsequent buoyancy-driven flow and heat transfer. The model calls for solution of the coupled two-dimensional equations of continuity, momentum, and energy with a one-dimensional radiative transfer model. After experimental validation of the model, parametric calculations were performed to determine the effect of the modified Rayleigh number, fluid Prandtl number, fluid layer opacity, cavity aspect ratio, opaque wall reflectivity, and convective heat loss from the transmitting wall. Natural convective motion and heat transfer are quite different from that found in cavities with differentially heated side walls. Results are presented in the form of temperature distributions, local heat transfer, contours of the stream function, and profiles of the predicted radiative flux divergence.

Nomenclature

A = aspect ratio of cavity, H/D
Bi = Biot number, $\bar{h}D/k$
D = fluid layer depth
F = local radiative flux
F^0 = radiative flux incident on vertical transparent wall
$\bar{h}$ = average heat-transfer coefficient at transmitting wall
H = fluid layer height
k = fluid thermal conductivity
Pr = Prandtl number, ν/α
q = convective heat flux
q^* = dimensionless convective heat flux, q/F^0
Ra^* = modified Rayleigh number, $g\beta F^0 D^4/k\nu\alpha$
T = local temperature
T_w = opaque wall temperature
T_∞ = ambient temperature
u = velocity in x direction
U = dimensionless velocity, uD/α
v = velocity in y direction
V = dimensionless velocity, vD/α
x = coordinate direction
y = coordinate direction
α = thermal diffusivity, $k/\rho c$
β = thermal expansion coefficient or intereflection function
η = dimensionless coordinate, y/D
θ = dimensionless temperature, $(T-T_w)/(F^0D/k)$
θ_∞ = dimensionless ambient temperature, $(T_\infty - T_w)/(F^0D/K)$
θ^0 = incidence angle for beam flux
κ = absorption coefficient of fluid
λ = wavelength
μ = direction cosine, $\cos\theta$
ν = kinematic viscosity
ξ = dimensionless coordinate, x/D
ρ_w = opaque wall reflectivity
$\rho^0(\mu^0)$ = directional reflectivity of transmitting interface in radiative flux model
τ = optical thickness
τ_D = fluid layer opacity
$\tau^0(\mu^0)$ = directional transmissivity of transmitting interface in radiative flux model, $1-\rho^0(\mu^0)$
Φ = dimensionless radiative flux, F/F^0
ψ = dimensionless stream function
ψ_c = absolute value of stream function at primary eddy center

Subscripts

b = beam component
d = diffuse component
w = opaque wall quantity
λ = spectral quantity

Superscripts

0 = incident flux quantity external to the system

Introduction

RADIATION-INDUCED buoyancy-driven flow is encountered in such diverse technologies as laser fusion, crystal growth, processing of semitransparent materials, advanced materials processing, photochemical reactions, and collection and utilization of solar energy. In such systems the primary driving force for the natural convective motion is the volumetric absorption of thermal radiation in semitransparent materials. The heat transfer and flow structure may be strongly affected by such variables as the magnitude of the external incident radiative flux and its spectral content, spectral absorption characteristics of the fluid, system geometry, reflectivity of solid surfaces forming enclosure, etc.

The purpose of this paper is to present the results of analytical work treating buoyancy-driven flow due to volumetric deposition of radiant energy in vertical rectangular enclosures. The problem of radiation/natural convection interaction in enclosures filled with a radiation participating fluid is one of a broader class of problems dealing with natural convective flow arising from arbitrary volumetric energy sources, a recent review of which is available.[1] Specifically, the interaction between radiation and natural convection in vertical slots and enclosures has been the subject of considerable research effort. The stability of vertical fluid layers as influenced by radiation absorption has been treated,[2,3] as well as the effect of radiation exchange between surfaces of an enclosure bounding a nonparticipating fluid.[4-6] Several recent investigations have treated the effects of radiation on the natural convective motion of a participating gas in rectangular enclosures.[7-11]

Received March 3, 1986; revision received May 8, 1986.

*Research Assistant, Heat Transfer Laboratory, School of Mechanical Engineering.

†W.F.M. Goss Distinguished Professor of Engineering, School of Mechanical Engineering. Associate Fellow AIAA.

All of the aforementioned investigations have treated the effects of radiation on fluid layers bounded by differentially heated walls, a situation in which buoyant enclosure flow exists anyway. This paper focuses on buoyancy-driven cavity flow arising solely from the volumetric deposition of radiant energy from an external source. A model is developed to predict the absorption of radiation by the fluid and the resulting steady-state natural convective motion. Results are presented in terms of temperature field, local heat transfer, flow structure, and profiles of the flux divergence as they are affected by the pertinent problem parameters.

Analysis

Physical Model

Consider a vertical layer of semitransparent fluid bounded on all sides by solid surfaces as shown in Fig. 1. One vertical wall is opaque and maintained at constant temperature, while the opposite vertical wall is transparent and serves to confine the fluid and transmit the external radiant energy incident upon it. The two horizontal bounding surfaces are assumed adiabatic. The radiation incident at $x=D$ penetrates the fluid layer and is absorbed, resulting in local volumetric heating and subsequent buoyancy-driven flow. The flow is assumed to be steady, two-dimensional, and laminar with constant properties. Additionally, the Boussinesq approximation is invoked, allowing for density variations in the field only insofar as they contribute to natural convective motion as a linearized function of temperature in the vertical component momentum equation.

Governing Equations

Introducing the dimensionless variables defined in the Nomenclature, the partial differential equations governing the transport of mass, momentum, and energy may be written as follows:

Mass:

$$\frac{\partial U}{\partial \xi}+\frac{\partial V}{\partial \eta}=0 \tag{1}$$

Momentum:

$$U\frac{\partial U}{\partial \xi}+V\frac{\partial U}{\partial \eta}=-\frac{\partial P}{\partial \xi}+Pr\left(\frac{\partial^2 U}{\partial \xi^2}+\frac{\partial^2 U}{\partial \eta^2}\right) \tag{2}$$

$$U\frac{\partial V}{\partial \xi}+V\frac{\partial V}{\partial \eta}=-\frac{\partial P}{\partial \eta}+Pr\left(\frac{\partial^2 V}{\partial \xi^2}+\frac{\partial^2 V}{\partial \eta^2}\right)+Ra^*Pr\theta \tag{3}$$

Energy:

$$U\frac{\partial \theta}{\partial \xi}+V\frac{\partial \theta}{\partial \eta}=\frac{\partial^2 \theta}{\partial \xi^2}+\frac{\partial^2 \theta}{\partial \eta^2}-\frac{d\Phi}{d\xi} \tag{4}$$

Note that the momentum and energy equations are coupled through the buoyancy and convective terms. As indicated by the total derivative of the dimensionless radiative flux $-d\Phi/d\xi$ and, as discussed later, the radiation field is assumed to be one-dimensional. The boundary conditions completing the specification of the hydrodynamic and thermal problem are stated as follows:

$$\eta=0: \quad U=V=\frac{\partial \theta}{\partial \eta}=0 \tag{5a}$$

$$\eta=A: \quad U=V=\frac{\partial \theta}{\partial \eta}=0 \tag{5b}$$

$$\xi=0: \quad U=V=\theta=0 \tag{5c}$$

$$\xi=1: \quad U=V=0, \ -\frac{\partial \theta}{\partial \xi}=Bi(\theta-\theta_\infty) \tag{5d}$$

The boundary condition at the transmitting wall $\xi=1$ [Eq. (5d)] implies 1) that conjugate effects in the transmitting vertical wall are neglected, i.e., that the wall is infinitely thin; and 2) that the transmitting wall is assumed to be perfectly transparent and absorbs none of the radiant energy incident upon it. More realistic treatments of this boundary are possible[12] and would be required in the rigorous modeling of a real physical system. However, the purpose of this study is to characterize the fluid flow and heat transfer due to direct deposition of radiation in the fluid-filled enclosure, for which this simplified boundary condition seems adequate.

Radiative Flux

An expression is required for the prediction of the radiative flux divergence $-d\Phi/d\xi$ in the energy equation (4) to complete the specification of the problem. To this end, several additional assumptions relative to the radiative transfer in the system are invoked. As stated earlier, radiant energy transfer is assumed to be one-dimensional. The fluid layer is assumed to be cold, an assumption justified by the fact that relatively low temperatures will be found in the system and that the emission will be in spectral regions where the fluid is effectively opaque. The external incident flux may be approximated as the sum of diffuse and beam components, $F^0=F_d^0+\mu^0 F_b^0$. Scattering in the fluid is assumed to be negligible. However, the model is also valid for radiant transfer in materials for which scattering is predominantly in the forward direction. The opaque wall of spectral reflectivity $\rho_{w\lambda}$ is assumed to be a diffuse reflector. Finally, all radiative properties are assumed to be independent of temperature. The model presented here for predicting the deposition of radiative flux was first formulated for the study of radiant transfer in stagnant horizontal layers of water[13] and was later validated experimentally.[14] The expressions for the spectral radiative flux and the flux divergence, as presented elsewhere,[13] and nondimensionalized here are, respectively,

$$\Phi_\lambda(\xi)=2[\tfrac{1}{2}\mu^0\tau^0(\mu^0)\Phi_{b\lambda}^0 e^{-(\tau_{D\lambda}-\tau_\lambda)/\mu}/\beta(\tau_{D\lambda},|\mu|) + \Phi_{d\lambda}^0 T_3(\tau_{D\lambda}-\tau_\lambda)-\Phi_{b\lambda}^* E_3(\tau_\lambda)] \tag{6}$$

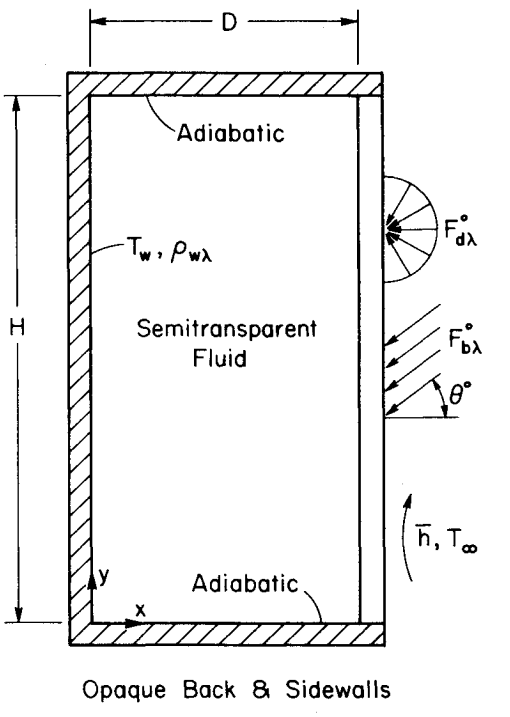

Fig. 1 Coordinate system and pertinent parameters.

and

$$-\frac{d\Phi_\lambda}{d\xi}=2\tau_{D\lambda}[\tfrac{1}{2}(\mu^0/\mu)\tau^0(\mu^0)\Phi^0_{b\lambda}e^{-(\tau_{D\lambda}-\tau_\lambda)/\mu}/\beta(\tau_{D\lambda},|\mu|)$$
$$+\Phi^0_{d\lambda}T_2(\tau_{D\lambda}-\tau_\lambda)+\Phi^*_{b\lambda}E_2(\tau_\lambda)] \quad (7)$$

where the flux at the opaque wall is given by

$$\Phi^*_{b\lambda}=2\rho_{w\lambda}[\tfrac{1}{2}\mu^0\tau^0(\mu^0)\Phi^0_{b\lambda}e^{-\tau_{D\lambda}/\mu}/\beta(\tau_{D\lambda},|\mu|)$$
$$+\Phi^0_{d\lambda}T_3(\tau_{D\lambda})] \quad (8)$$

The fluid layer opacity, exponential and transmission integrals, and interreflection function are given, respectively, by

$$\tau_\lambda=\int_0^x\kappa_\tau dx \quad (9a)$$

$$\tau_{D\lambda}=\int_0^D\kappa_\lambda dx \quad (9b)$$

$$E_n(x)=\int_0^1 e^{-x/\mu}\mu^{n-2}d\mu \quad (9c)$$

$$T_2(x)=\int_0^1\tau^0(\mu')e^{-x/\mu}(\mu'/\mu)d\mu'/\beta(\tau_D,|\mu|) \quad (9d)$$

$$T_3(x)=\int_0^1\tau^0(\mu')e^{-x/\mu}\mu'd\mu'/\beta(\tau_D,|\mu|) \quad (9e)$$

$$\beta(\tau_D,|\mu|)=1-\rho_{w\lambda}\rho(\mu)e^{-2\tau_D/|\mu|} \quad (9f)$$

Under the framework of the simplied transmitting wall boundary condition presented earlier, the surface reflectivity $\rho^0(\mu^0)$ is assumed to vanish and, consequently, $\tau^0(\mu^0)=1$. Then, the transmission integral functions $T_2(x)$ and $T_3(x)$ reduce to exponential integral functions of the same order. These simplifications reduce the number of parameters of the problem without altering the basic physics of interest here. Notice that the dimensionless diffuse incident flux $\Phi^0_{d\lambda}$ represents the fraction of total incident flux that is diffuse. Once $\Phi^0_{d\lambda}$ and μ^0 are specified, the dimensionless beam component is not independent, since

$$\Phi^0_{b\lambda}=(1-\Phi^0_{d\lambda})/\mu^0 \quad (10)$$

The singularity as μ^0 approaches zero is not of interest since the collimated flux would then be directed parallel to the vertical wall and would not contribute to the volumetric deposition of the radiation.

Method of Solution

The conservation equations of mass, momentum, and energy, and their boundary conditions [Eqs. (1-5)], along with the expression for the radiative flux divergence [Eq. (7)], complete the mathematical formulation of the problem. A closed-form analytical solution is not possible. The equations were therefore solved numerically. The control-volume scheme of Patankar[15] was used to discretize the governing equtions. The SIMPLER algorithm[15] was employed to treat the coupling between pressure and momentum. A grid size study was conducted on computational meshes ranging from 16×16 to 42×42, after which a 32×32 nonuniform grid was selected for the parametric calculations. The difference in total heat transfer to the cooled wall and maximum stream function was less than 1% between the 32×32 and 42×42 grid. Nodes were clustered near the solid walls in order to resolve the fine thermal and velocity boundary layers there. The clustering of nodes near the transmitting wall was also important in the calculation of the local volumetric rate of radiation absorption for high fluid layer opacities where the radiative flux is attenuated in a small fraction of the layer depth. Iterations were terminated when the radiant energy deposition integrated over the fluid layer matched the sum of the heat transfer by convection to the isothermal wall and the heat loss to the ambient from the transmitting wall to within 0.1%.

Results and Discussion

Model Validation

The model outlined in the foregoing paragraphs (with a more rigorous treatment of the transmitting wall boundary condition) has been verified experimentally, the details of which can be found elsewhere.[12] Briefly, a cavity containing pure water was exposed to irradiation of known spectral flux. A Mach-Zehnder interferometer was used to measure the temperature distribution in the liquid. Flow visualization was performed by injection of a fluorescing tractor, which was then exposed to a sheet of laser light. Interferograms and results of the flow visualization were recorded photographically and compared to predictions with local flux divergence calculations performed on a spectral basis. Spectral calculations were required because the absorption coefficient for water varies nearly six orders of magnitude in a wavelength range of 0.3-2.4 μm.[16] Figure 2 shows the predicted and experimentally measured temperature profile at the test cell vertical centerline ($\xi=\frac{1}{2}$), for $Ra^*=2.26\times10^8$ and $A=2.0$. The agreement between predictions and data is seen to be very good except near $\eta=2.0$, where heat loss and possible free surface effects were present. The maximum discrepancy is still less than 15%. Extremely high interference fringe density at the cooled wall made measurement of temperatures in the boundary layer and, hence, determination of the local heat transfer impossible.

Despite such high Rayleigh number, unsteadiness in the flow was not observed experimentally. A laminar character prevailed throughout the flowfield. The predicted flow structure and results of the flow visualization experiments (not shown) were also in good agreement. The details of the experiment with results of the flow visualization and interferometry, along with the treatment of the transmitting wall boundary condition employed in the analysis are given elsewhere.[12]

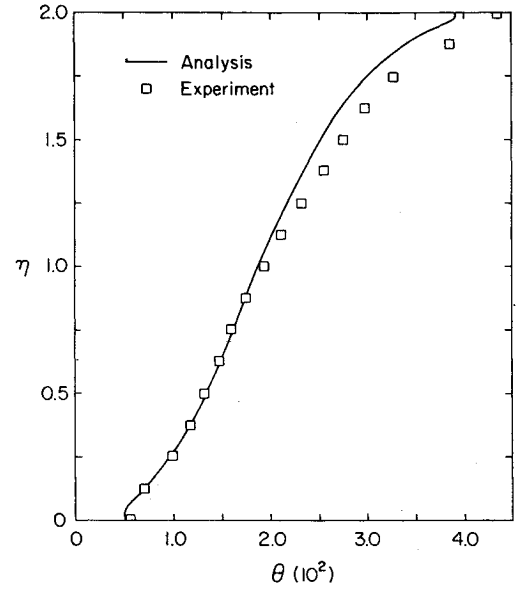

Fig. 2 Comparison of predicted and experimentally determined vertical temperature profile at $\xi=\frac{1}{2}$ for water, $Ra^*=2.26\times10^8$, and $A=2.0$.

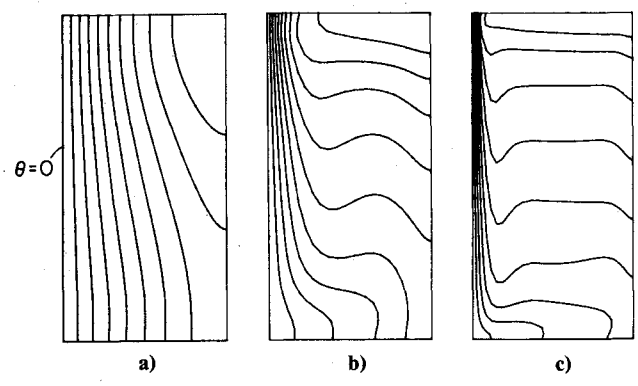

Fig. 3 Effect of Rayleigh number in the temperature distribution, $Pr = = 6.0$, $Bi = 0$, $A = 2.0$, $\rho_w = 0$, and $\Delta\theta = \theta_{max}/10$: a) $Ra^* = 10^3$, $\theta_{max} = 0.395$; b) $Ra^* = 10^5$, $\theta_{max} = 0.191$, c) $Ra^* = 10^7$, $\theta_{max} = 0.072$.

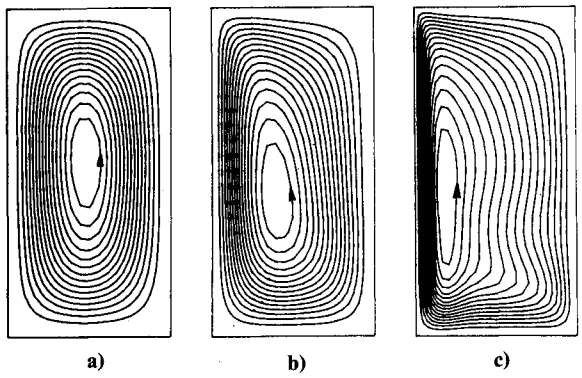

Fig. 4 Effect of Rayleigh number on flow structure for the same conditions as Fig. 3, $\Delta\psi = \psi_{max}/16$: a) $Ra^* = 10^3$, $\psi_{max} = 0.9$; b) $Ra^* = 10^5$, $\psi_{max} = 9.5$; c) $Ra^* = 10^7$, $\psi_{max} = 29.4$.

Model Parameters

Examination of the governing equations and boundary conditions [Eqs. (1-5)] reveals the following pertinent problem parameters: Ra^*, Pr, Bi, θ_∞, and A. Additionally, the radiation facet of the problem introduces the parameters $\rho_{w\lambda}$, μ^0, $\Phi_{d\lambda}$, and $\tau_{D\lambda}$. Calculations have been performed to determine the effects of these parameters on the resulting distribution of the radiative flux divergence, local heat transfer at the opaque isothermal wall, temperature distribution, and flow structure. Simulations were made in the ranges $10^3 \le Ra^* \le 10^8$, $0.01 \le Pr \le 1000$, $1 \le A \le 5$, and $0 \le Bi \le 5.0$ for $\theta_\infty = 0$. The effect of the radiation parameters was studied for $0.1 \le \tau_D \le 100.0$, and $\rho_w = 0$ and 1.0 for $\mu^0 = 10$ and $\Phi_{d\lambda} = 0$. Radiation was treated on a gray basis. A base set of parameters was established and values were perturbed about the base case to determine the effect of each parameter independently. The parameters for the base case were $Ra^* = 10^6$, $Pr = 6.0$, $A = 2.0$, $Bi = 0$, $\tau_D = 1.0$, and $\rho_w = 0$. All calculations were perfomred for $\mu^0 = 1.0$ and $\Phi_d = 0$, i.e., for flux entirely collimated at normal incidence. Previous studies have shown that results are insensitive to the partitioning between collimated and diffuse radiative flux components as long as the magnitude of the total flux incident on the boundary remains the same.[13] Results representative of the effects of the parameters studied are presented in sections to follow. The reader is referred to Ref. 12 for a detailed presentation and discussion of the results.

Effect of Modified Rayleigh Number

The effect of the modified Rayleigh number Ra^* was determined by performing calculations for $Ra^* = 10^3$, 10^4, 10^5, 10^6, 10^7, and 10^8. Care was taken at the highest Rayleigh number to ensure that there was adequate resolution in the boundary layer. Representative predicted temperature distributions are shown in Fig. 3, where the equal division between adjacent isotherms is $\Delta\theta = \theta_{max}/10$. The cooled wall is on the left and the transmitting wall on the right. Some interesting trends are observed. It appears that three distinct regimes emerge as the Rayleigh number is increased. The conduction regime is apparent for $Ra^* < 10^3$, where the isotherms tend to be vertical and more parallel. The effect of the flow is felt only minimally. As Ra^* increases, the thermal boundary layer becomes thinner at the isothermal wall and the vertical character of the isotherms in the enclosure center breaks down. This may be termed transition where conduction becomes less important and the flow intensifies. Finally, the boundary-layer regime emerges near $Ra^* = 10^5$. Here, convection is clearly the dominant mode of heat transfer as the thermal boundary is very thin along the cooled wall, particularly near the top ($\eta = A$) where the warm fluid impinges against the cold surface. The core appears as stagnant and thermally stratified, with the warm, less dense fluid above the cooler, more dense fluid. The vertical temperature gradient in the stagnant core appears almost linear for $Ra^* = 10^7$. The appearance of these three regimes is similar to that found in cavity flows with differentially heated end walls.[17] The natural convection circulation and heat transfer also showed conduction/transition/convection development with increasing Rayleigh number in cavities with spatially uniform internal energy sources.[1] A more direct comparison is not possible, however, due to the highly nonuniform internal radiative heating and different boundary condition studied here. Nevertheless, it is significant that three distinct regimes have also been observed for flow induced solely by volumetric deposition of radiation.

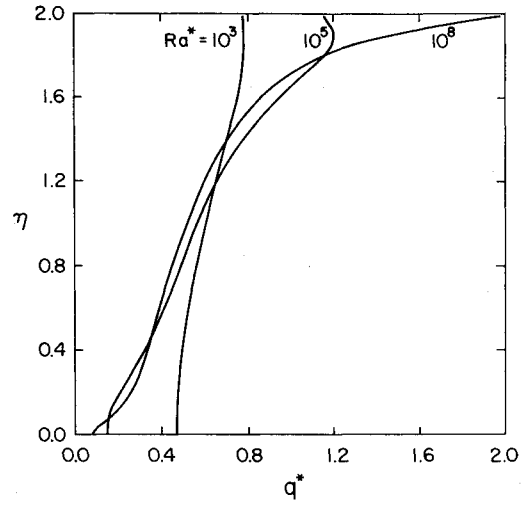

Fig. 5 Local convective heat flux at the isothermal wall for $Ra^* = 10^3$, 10^5, and 10^8 (conditions same as Fig. 3).

The experimental prescription of a critical modified Rayleigh number at which transition to turbulent flow occurs for the physical system modeled here has not been addressed in the literature. The Rayleigh number corresponding to transition to turbulent natural convection in a cavity with differentially heated walls clearly does not apply, since the basic physics for the buoyancy-induced motion are not the same. As explained in the seciton outlining validation of the theoretical model, the result of the experimental flow visualization and interferometric study showed no indication of flow unsteadiness or turbulence in water at $Ra^* = 2.26 \times 10^8$. This is further supported by the fact that predictions of the laminar flow model presented here showed good agreement with the experimentally measured temperature distribution and flow structure.[12] Therefore, the results of predictions for modified

Table 1 Effect of modified Rayleigh number on stream function at eddy center ($Pr=6$, $\tau_D=1$, $A=2$, $Bi=0$, $\rho_w=0$)

Ra^*	ψ_c	Ra^*	ψ_c
10^3	0.9	10^6	17.4
10^4	3.9	10^7	29.4
10^5	9.5	10^8	49.6

Rayleigh numbers up to $Ra^*=10^8$ presented here can be accepted with confidence.

The dimensionless stream function was calculated from the converged velocity fields by means of the pair of equations

$$\psi_{\xi,\eta=0}=\psi_{\xi=0,\eta=0}-\int_0^{\xi} V\mathrm{d}\xi \tag{11}$$

$$\psi_{\xi,\eta}=\psi_{\xi,\eta=0}+\int_0^{\eta} U\mathrm{d}\eta \tag{12}$$

where $\psi_{\xi=0,\eta=0}$ was arbitrarily taken to be zero. The stream function contours for increasing Ra^* corroborate the existence of the regimes discussed in the foregoing. As seen in Fig. 4, the flow intensifies as Ra^* increases. Also, the flow structure loses completely the centrosymmetry characteristic of constant property flow in a cavity with differentially heated side walls. The eddy center is displaced close to the cooled wall as it is there that the velocity boundary layer thins. The curious "humps" in the ψ contours seen for $Ra^*=10^7$ at the bottom and side are the result of the natural mechanism for momentum exchange from thin to thicker boundary layers as the flow turns the corners. The intensity of the flow can be measured by the absolute value of the dimensionless stream function at the eddy center ψ_c. This value reflects the mass flow rate in the boundary layer. Table 1 illustrates the increased intensity of the natural convective motion with increased Rayleigh number. The flow is relatively stagnant at the lower Rayleigh numbers and the increasing Ra^* results in radically higher ψ_c.

The local dimensionless convective heat flux at the isothermal wall as a function of vertical height is shown for $Ra^*=10^3$, 10^5, and 10^8 in Fig. 5. The convective heat flux was calculated from the converged temperature field by means of the definition,

$$q^*(\eta)=-\left.\frac{\partial\theta}{\partial\xi}\right|_{\xi=0} \tag{13}$$

The results are presented in terms of heat flux rather than a local Nusselt number because there is no unique reference temperature on which to base the Nusselt number. Note that, since the fluid layer opacity is the same for the three Rayleigh number simulations, the total radiant energy deposited in the fluid is the same and, hence, $\int_0^A q^*(\eta)\mathrm{d}\eta=\text{const}$. The heat flux varies little along the wall for the lowest Rayleigh number, characteristic of conduction-dominated heat transfer. As the boundary-layer flow structure develops, the local heat flux becomes more nonuniform. The fluid in the boundary layer heated by absorption of radiation impinges against the cooled wall near $\eta=A$, resulting in very high local heat-transfer rate at that point. The greatest variation is seen for $Ra^*=10^8$, where convection clearly dominates.

Variations of the thermophysical properties with temperature, which may become important at higher Rayleigh numbers, were not included in the analysis. The maximum temperature difference observed in the experiments conducted was 5°C.[12] Consequently, a variable property model was not warranted. The influence of variable properties on the heat transfer and natural convective motion in a differentially heated square enclosure has recently been studied; the reader is referred to Ref. 18 for a discussion of the effects.

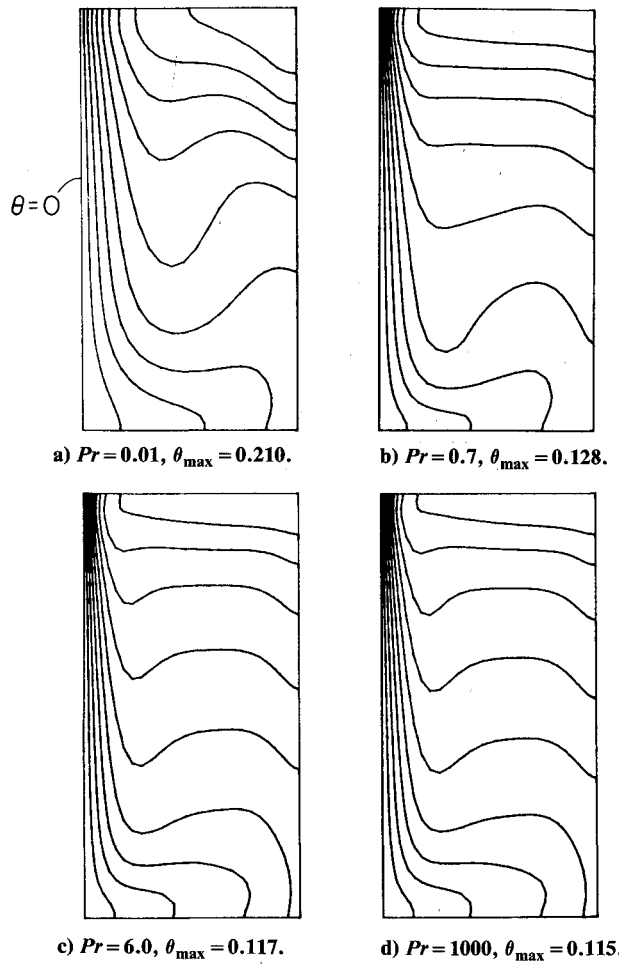

a) $Pr=0.01$, $\theta_{max}=0.210$. b) $Pr=0.7$, $\theta_{max}=0.128$.

c) $Pr=6.0$, $\theta_{max}=0.117$. d) $Pr=1000$, $\theta_{max}=0.115$.

Fig. 6 Effect of fluid Prandtl number on the temperature distribution, $Ra^*=10^6$, $Bi=0$, $A=2.0$, $\tau_D=1.0$, $\rho_w=0$, $\Delta\theta=\theta_{max}/10$.

Effect of Fluid Prandtl Number

Calculations were performed for fluid Prandtl numbers of 0.01, 0.7, 6.0, 50.0, and 1000.0 in an effort to simulate representative semitransparent fluids such as semiconductors, gases, water, paraffins, and viscous oils, respectively. Most low Prandtl number fluids are liquid metals and are opaque, subject only to surface radiative heating. However, semiconductors also have characteristically low Prandtl numbers and are semitransparent to thermal radiation.

Temperature distributions are shown in Fig. 6 for the different Prandtl numbers studied. The thermal boundary layer thins as the Prandtl number increases. It should be noted that the maximum dimensionless temperature increases with Pr as well. Convection becomes more important and the boundary-layer regime is promoted by higher Pr. All of these phenomena can be attributed to the very high thermal conductivity characteristic of most low Prandtl number fluids. The heat-transfer rate is expected to be less convection dominated for fluids having high thermal conductivity. This is corroborated by a comparison of the stream function at the eddy center where ψ_c values are 9.1, 18.4, 17.4, 17.3, and 17.3 for $Pr=0.01$, 0.7, 6.0, 50.0, and 1000.0, respectively, at $Ra^*=10^6$, $\tau_D=1.0$. Mass flow in the boundary layer for the low Prandtl number fluid is nearly half that found in the more convection-dominated high Pr simulations. Also of note is the weak maximum in the $Pr-\psi_c$ relationship somewhere near $Pr=0.7$. The dependence of the flow structure on Pr is strongest below $Pr=6.0$, as seen in Fig. 7. Above this value, the viscous forces have reached a point where further increases in Pr result in no change in the temperature distribution and flowfield. Weak secondary eddies are found in all four corners

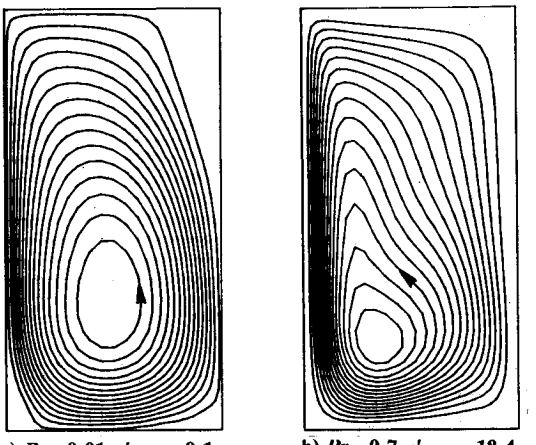

a) $Pr=0.01$, $\psi_{max}=9.1$. b) $Pr=0.7$, $\psi_{max}=18.4$.

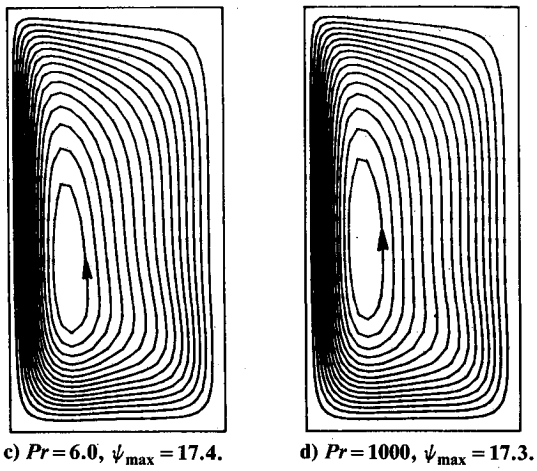

c) $Pr=6.0$, $\psi_{max}=17.4$. d) $Pr=1000$, $\psi_{max}=17.3$.

Fig. 7 Effect of Prandtl number on flow structure, same conditions as Fig. 6, $\Delta\psi=\psi_{max}/16$.

for $Pr=0.01$, with a sizeable eddy near $\xi=1$ and $\eta=A$, but their effect on local heat-transfer rate is small since the conduction is so strong. Secondary recirculation cells were also observed at low Pr in a numerical study of natural convection in enclosures with uniform internal heating.[1]

Effect of Fluid Layer Opacity

Profiles of the radiation flux divergence for the fluid layer opacities studied of 0.1, 1.0, 10.0, and 100.0 are plotted in Fig. 8. The profile ranges from nearly uniform weak deposition for $\tau_D=0.1$ to very high deposition only in the fluid layers adjacent to the transmitting wall for $\tau_D=100.0$. Note that the maximum radiation flux divergence for $\tau_D=100.0$ is eight times greater than for $\tau_D=10.0$. As the opacity increases, the volumetric rate of radiant energy deposition approaches a uniform heat flux boundary condition at $\xi=1$. The effect of the highly nonuniform spatial distribution of the volumetric energy source can be seen in the temperature profiles at the midplane. See Fig. 9. Greater deposition of energy near $\xi=1$ for increasing τ_D causes the higher temperatures near the transmitting wall. In the limit, as $\tau_D\to\infty$, the boundary condition at $\xi=1$ corresponds to constant heat flux input. Accordingly, an increased fluid layer opacity promotes formation of a thermal boundary layer there. The corresponding stream function contours of Fig. 10 support this observation. As the opacity is increased, the hydrodynamic boundary layers along both vertical walls become thinner and the stagnant central core expands to occupy more of the cavity. The maximum stream function increases from 0.1 for $\tau_D=0.1$ to 19.3 for $\tau_D=10.0$ as both the magnitude and spatial nonuniformity of

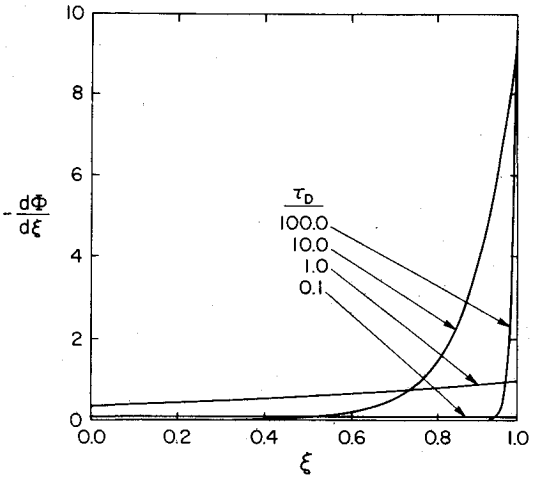

Fig. 8 Profiles of the radiative flux divergence for $\tau_D=0.1$, 1.0, 10.0, and 100.0 (⅛ scale for $\tau_D=100.0$).

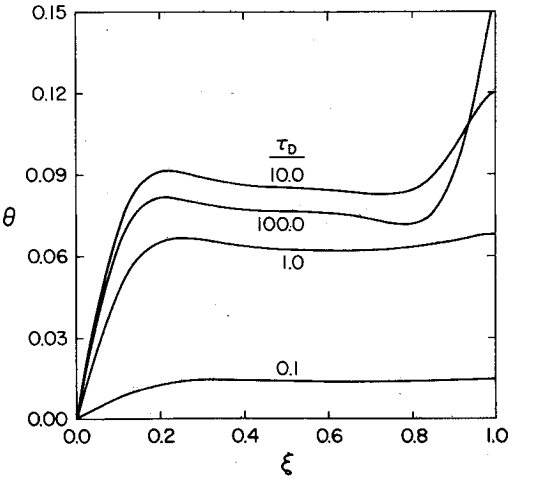

Fig. 9 Temperature profiles at the midplane $\eta=1$ for $\tau_D=0.1$, 1.0, 10.0, and 100.0 ($Ra^*=10^6$, $Pr=6.0$, $Bi=0$, $A=2.0$, and $\rho_w=0$).

the flux divergence increase. At $\tau_D=100.0$, the maximum stream function is 16.5, a decrease from the value at $\tau_D=10.0$. The fluid layer is so opaque for $\tau_D=100.0$ that the radiation is not able to penetrate and buoyantly lift the fluid throughout the enclosure, as is possible for lower τ_D. This results in the observed decrease in ψ_c and the lower temperature in the core for $\tau_D=100.0$ seen in Fig. 9.

Effect of Opaque Wall Reflectivity

Computations for the cases of perfectly black ($\rho_w=0$) and perfectly reflecting ($\rho_w=1.0$) opaque walls revealed no discernible visual difference in the temperature distributions and flowfields for the base case parameters of $Ra^*=10^6$, $\tau_D=1.0$, and $Pr=6.0$. The mass flow in the boundary layer increased only marginally from $\psi_c=17.4$ to 17.9 as the reflectivity was increased from zero to unity. This marginal difference is not unexpected for the $\tau_D=1.0$ case studied. Fluid layers of lower opacity are expected to be influenced more by the opaque wall reflectivity since the deposition of the incident flux may be augmented by reflection for $\rho_w=1.0$. For highly reflecting walls, however, much of the radiant energy may be reflected back through the transmitting wall and lost from the system. The flow and heat transfer are expected to be influenced even less for higher τ_D as absorption in the fluid causes complete attenuation of the incident flux for $\tau_D>10.0$ before reaching the opaque walls (see Fig. 8).

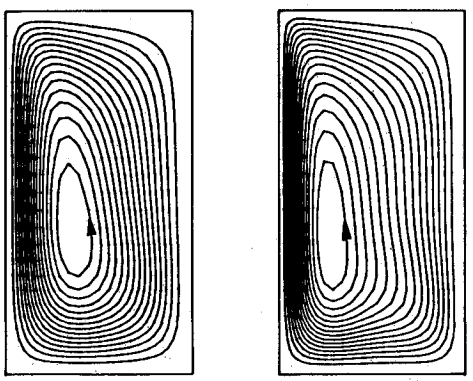

a) $\tau_D = 0.1$, $\psi_{max} = 10.0$. b) $\tau_D = 1.0$, $\psi_{max} = 17.4$.

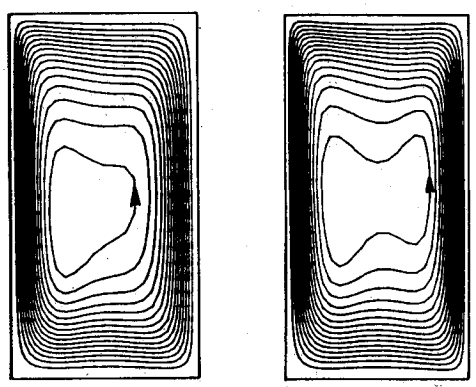

c) $\tau_D = 10.0$, $\psi_{max} = 19.3$. d) $\tau_D = 100.0$, $\psi_{max} = 16.5$.

Fig. 10 Effect of fluid layer opacity on flow structure, same conditions as Fig. 9, $\Delta\psi = \psi_{max}/16$.

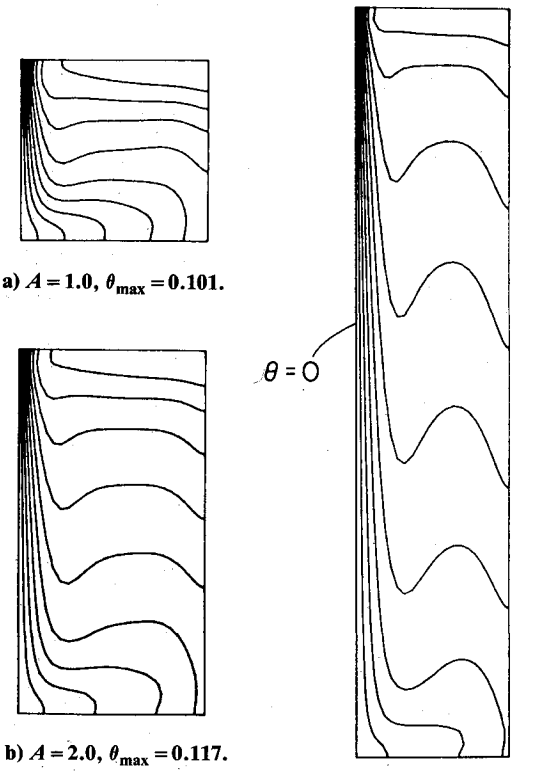

a) $A = 1.0$, $\theta_{max} = 0.101$.

b) $A = 2.0$, $\theta_{max} = 0.117$.

c) $A = 5.0$, $\theta_{max} = 0.139$.

Fig. 11 Temperature distributions as affected by enclosure aspect ratio, $Ra^* = 10^6$, $Pr = 6.0$, $Bi = 0$, $\tau_D = 1.0$, $\rho_w = 0$, $\Delta\theta = \theta_{max}/10$.

Effect of Enclosure Aspect Ratio

The temperature distributions for cavities of aspect ratio $A = 1.0$, 2.0, and 5.0 are presented in Fig. 11. The maximum fluid temperature in the cavity was observed to increase with aspect ratio. This is caused by higher area exposed to the incident flux for increasing A. The central core is seen to be less stagnant in cavities of larger aspect ratio, as shown by the tendency toward a nonhorizontal temperature profile there. The increasingly nonhorizontal isotherms in the central core for slender cavities have been observed experimentally and predicted previously,[19,20] producing multiple secondary vortices there for moderate Rayleigh numbers and high aspect ratios. The maximum stream function corresponding to the three aspect ratios was 11.1, 17.4, and 34.3 for $Ra^* = 10^6$, $\tau_D = 1.0$, and $Pr = 6.0$. The increase in ψ_c with increasing aspect ratio is the result of higher total radiant energy deposition and greater cooled wall length for inducing fluid motion. Stream function contours (not shown) exhibit a general vertical "stretching" of the flow structure as the aspect ratio is increased.

Effect of Convective Heat Loss from Transmitting Wall

Simulations were carried out for $Bi = 0$, 0.5, and 5.0 with $\theta_\infty = 0$ to determine the influence of convective heat loss from the transmitting wall on flow and temperature fields. The results for $Bi = 0.5$ and 5.0 are shown in Figs. 12a and 12b, respectively. In general, the effect of heat loss to the ambient is to reduce the intensity of the flow. The magnitude of ψ_c for $Bi = 0$, 0.5, and 5.0 was 17.4, 17.3, and 16.1, respectively, at $Ra^* = 10^6$, $\tau_D = 1.0$, and $Pr = 6.0$. The ratio of heat loss by convection to total radiant energy deposited was 0, 0.053, and 0.29, respectively. Heat loss is so high for $Bi = 5.0$ that a radical reversal of isotherms is present, resulting in a large counterrotating secondary eddy over 70% of the height of the transmitting wall. The deposition of radiation is still large

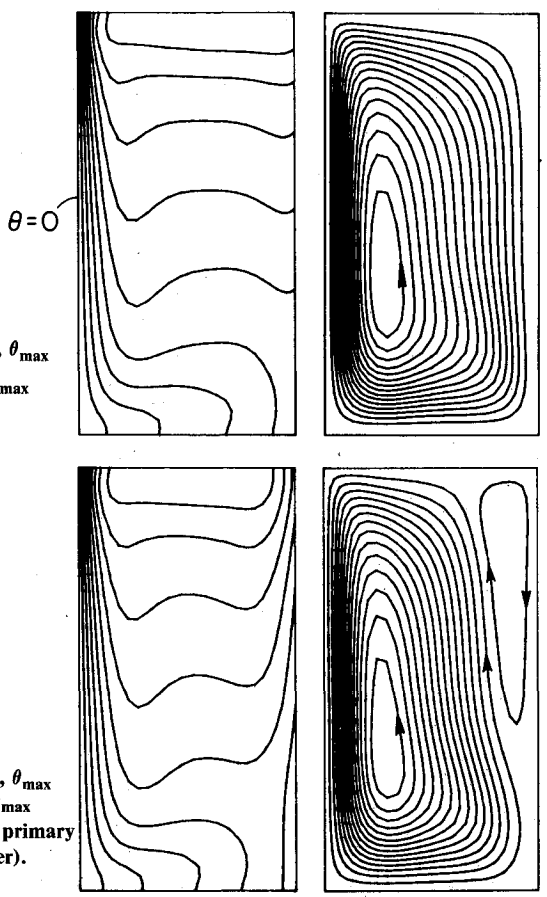

a) $Bi = 0.5$, $\theta_{max} = 0.108$, $\psi_{max} = 17.3$.

b) $Bi = 5.0$, $\theta_{max} = 0.082$, $\psi_{max} = 16.1$ (at primary eddy center).

Fig. 12 Effect of convective heat loss on temperature distribution and flow pattern for $Ra^* = 10^6$, $Pr = 6.0$, $\theta_\infty = 0$, $A = 2.0$, $\tau_D = 1.0$ $\rho_w = 0$, $\Delta\theta = \theta_{max}/10$, $\Delta\psi = \psi_{max}/16$.

enough, however, to buoyantly lift the flow on the interior of the cavity.

Conclusions

An analysis has been presented for the prediction of direct deposition of radiant energy in a vertically oriented fluid layer and the resulting natural convective motion in rectangular enclosures. The most important parameters affecting the natural convection circulation and heat transfer appear to be the Rayleigh number, fluid Prandtl number, and fluid layer opacity. Calculations show generally that fluid flow and heat transfer are markedly different from that characteristic of cavities with differentially heated side walls. The flow structure loses completely its centrosymmetry especially at high Rayleigh numbers. Except for very opaque fluid layers, a thermal boundary layer is formed only at the cooled opaque wall. In the limit as $\tau_D \to \infty$, the boundary on which the radiation is incident corresponds to a constant heat flux boundary condition. The driving force for radiation-induced natural convection heat transfer is thus quite different than for differentially heated cavities.

Results from parametric calculations reveal the existence of conduction, transition, and boundary-layer regimes as the modified Rayleigh number is increased. Computations for fluid Prandtl numbers of 0.01–1000 illustrate the dominance of convection for high *Pr* fluids, whereas conduction appears of greater importance for low Prandtl number fluids. An increase in the fluid layer opacity promotes the formation of a boundary layer near the transmitting wall where very high volumetric energy deposition occurs. Enclosures with higher aspect ratios result in less stagnant central core in the boundary-layer regime. Finally, a decrease in the convective heat loss and an increase in opaque wall reflectivity intensify the flow, although the effect is slight.

No mention has been made of the effects of multiple components in the system where the absorption of radiant energy is strongly dependent on local species concentration. In this case, the coupling is stronger between the rate of volumetric energy deposition in the fluid and the thermally and solutally driven convection. Such is the case in most of the applications listed in the Introduction and, consequently, further research is needed.

Acknowledgment

Author Webb wishes to acknowledge support of his graduate studies by an Eastman Kodak Co. Graduate Fellowship. Computer facilities were made available by the Purdue University Computing Center.

References

[1]Kulacki, F. A. and Richards, D. E., "Natural Convection in Plane Layers and Cavities with Volumetric Energy Sources," *Natural Convection Fundamentals and Applications*, edited by S. Kakac, W. Aung, and R. Viskanta, Hemisphere, Washington, DC, 1985, pp. 179-255.

[2]Hassab, M. A. and Ozisik, M. N., "Effects of Radiation and Convective Boundary Conditions on the Stability of Fluid in an Inclined Slender Slot," *International Journal of Heat and Mass Transfer*, Vol. 22, July 1979, pp. 1095-1105.

[3]Arpaci, V. S. and Bayazitoglu, Y., "Thermal Stability of Radiating Fluids: Asymmetric Slot Problem," *The Physics of Fluids*, Vol. 16, May 1973, pp. 589-593.

[4]Kim, D. M. and Viskanta, R., "Effect of Wall Conduction and Radiation on Natural Convection in a Rectangular Cavity," *Numerical Heat Transfer*, Vol. 7, Oct.-Dec. 1984, pp. 449-470.

[5]Kim, D. M. and Viskanta, R., "Heat Transfer by Conduction, Natural Convection, and Radiation Across a Rectangular Cellular Structure," *International Journal of Heat Fluid Flow*, Vol. 5, Dec. 1984, pp. 205-213.

[6]Larson, D. W. and Viskanta, R., "Transient Combined Laminar Free Convection and Radiation in a Rectangular Enclosure," *Journal of Fluid Mechanics*, Vol. 78, Nov. 1976, pp. 65-85.

[7]Desrayand, G. and Lauriat, G., "Natural Convection of a Radiating Fluid in a Vertical Layer," *Transactions of ASME, Journal of Heat Transfer*, Vol. 107, Aug. 1985, pp. 710-712.

[8]Shih, T. M. and Ren, A. L., "Combined Convective and Radiative Recirculating Flows in Enclosures," *Natural Convection in Enclosures—1983*, edited by I. Catton and K. E. Torrance, ASME, New York, 1983, pp. 49-57.

[9]Chang, L. C., Yang, K. T., and Lloyd, J. R., "Radiation-Natural Convection Interactions in Two-Dimensional Complex Enclosures," *Transactions of ASME, Journal of Heat Transfer*, Vol. 105, Feb. 1983, pp. 89-95.

[10]Lauriat, G., "Combined Radiation-Convection in Gray Fluids Enclosed in Vertical Cavities," *Transactions of ASME, Journal of Heat Transfer*, Vol. 104, 1982, pp. 609-615.

[11]Lauriat, G., "Numerical Study of the Interaction of Natural Convection With Radiation in Nongray Gases in a Narrow Vertical Cavity," *Heat Transfer—1982,* Vol. 2, Hemisphere, Washington, DC, 1982, pp. 153-158.

[12]Webb, B. W., "Radiation-Induced Natural Convection and Melting of Semitransparent Materials," Ph.D. Thesis, Purdue University, West Lafayette, IN, August 1986.

[13]Viskanta, R. and Toor, J.S., "Radiant Energy Transfer in Waters," *Water Resources Research*, Vol. 8, June 1972, pp. 595-608.

[14]Snider, D. M. and Viskanta, R., "Radiation-Induced Thermal Stratification in Surface Layers of Stagnant Water," *Transaction of ASME, Journal of Heat Transfer*, Vol. 97, Feb. 1975, pp. 35-39.

[15]Patankar, S. V., *Numerical Heat Transfer and Fluid Flow*, McGraw-Hill Book Co., New York, 1980.

[16]Hale, G. M. and Querry, M. R., "Optical Constants of Water in the 200-nm to 200-μm Wavelength Region," *Applied Optics*, Vol. 12, March 1973, pp. 555-563.

[17]Bejan, A., *Convection Heat Transfer*, John Wiley & Sons, New York, 1984, Chap. 5.

[18]Zhong, Z. Y., Yang, K. T., and Lloyd, J. R., "Variable Property Effects in Laminar Natural Covnection in a Square Enclosure," *Transactions of ASME, Journal of Heat Transfer*, Vol. 107, Feb. 1985, pp. 133-138.

[19]Elder, J. W., "Laminar Free Convection in a Vertical Slot," *Journal of Fluid Mechanics*, Vol. 23, Sept. 1965, pp. 77-98.

[20]Pepper, D. W. and Harris, S. D., "Numerical Simulation of Natural Convection in Closed Containers by a Fully Implicit Method," *Transactions of ASME, Journal of Fluids Engineering,* Vol. 99, Dec. 1977, pp. 649-656.